Available online at www.sciencedirect.com
ScienceDirect
Procedia Engineering 2 (2010) 1961–1971
Procedia Engineering
www.elsevier.com/locate/procedia

Fatigue 2010

In-situ characterization of the microstructure evolution during cyclic deformation of novel cast TRIP steel

A. Weidner *, A. Glage, H. Biermann

Institute of Materials Engineering, Technische Universität Bergakademie Freiberg, Gustav-Zeuner-Str. 5, 09599 Freiberg, Germany

Received 4 March 2010; revised 10 March 2010; accepted 15 March 2010

Abstract

In-situ investigations of the cyclic deformation behavior of a metastable high-alloyed austenitic stainless cast TRIP-steel (TRIP – effect; TRansformation Induced Plasticity) in a scanning electron microscope (SEM) are presented. Low cycle fatigue (LCF) tests of the metastable cast steel alloy at different strain amplitudes showed that three different kinds of cyclic softening/hardening behaviour can be distinguished caused by different microstructures. In-situ push-pull tests in the SEM at two different applied total strain amplitudes were carried out showing the evolution of the microstructure in dependence on the number of cycles. The phase transformation of the metastable austenite to the α'-martensite and changes in the microstructure (deformation bands, dislocation arrangements) were investigated applying different SEM techniques as electron backscatter diffraction (EBSD) and electron channelling contrast imaging (ECCI). It is shown that the formation of deformation bands starts just from the beginning of the cyclic deformation and almost as multiple slip. ECC images show that these bands consist of very fine, elongated lamellas with increasing density and length at increasing number of cycles. Many of these fine lamellas grow together and form the deformation bands. The lamellas can be correlated with stacking faults. At a certain thickness the deformation bands were identified by EBSD as a hexagonal crystal structure. For the two applied total strain amplitudes different microstructures were observed regarding both the amount of martensite phase transformation as well as the dislocation arrangements.

Keywords: In-situ deformation; deformation bands; martensitic transformation; EBSD; ECCI

1. Introduction

Recently, a new generation of metal matrix composites was created by the collaborative research centre "TRIP-Matrix-Composites" (TRIP…TRansformation Induced Plasticity) founded by the German Research Foundation at the Technical University Freiberg [1]. A steel matrix composite material was designed on the basis of metastable austenitic cast steel [2] and MgO partially stabilized ZrO_2. Both phases undergo a martensitic phase transformation during plastic deformation resulting in high strength and high uniform elongation for maximum of energy absorption. The metastable austenitic steel shows a phase transformation from fcc to bcc structure. The MgO-ZrO_2

* Corresponding author. Tel.:+49 3731 39 2124; fax: +49 3731 39 3703.
E-mail address: weidner@ww.tu-freiberg.de

1877-7058
doi:10.1016/j.proeng.2010.03.211

shows a phase transformation from tetragonal to monocline structure. From the combination of both phase transformation effects new high quality properties are expected. The new material will be manufactured either by infiltration of ceramic preforms (foam or porous ceramic bodies) or on a powder metallurgical path by extrusion and sintering procedures. First results on prototypes with regard to the properties of this new type of composite materials were already published elsewhere [3, 4]. In the future, further detailed investigations of the mechanical properties, the real structure and the structure-property relations are performed. This includes investigations of the static, dynamic, cyclic and multiaxial deformation behavior. To study the evolution of microstructure, scanning electron microscopy, computer tomography and X-ray diffractometry during in-situ deformation are applied.

First of all, careful studies of the mechanical behavior and microstructure development in the TRIP-steel matrix are necessary. First results on static, dynamic and cyclic deformation behavior in combination with microstructural observations were already published elsewhere [5-7]. Studies of the cyclic deformation behavior of a high-alloyed metastable austenitic stainless cast steel [6, 7] revealed combinations of cyclic hardening, saturation and cyclic softening caused by the presence or absence of a martensitic phase transformation depending on the applied cyclic total strain amplitude. Investigations of the dislocation arrangement on samples deformed to failure have shown that at low strain amplitudes planar dislocation structures predominate, whereas at high strain amplitudes cells/walls develop.

The aim of the present study is to follow the evolution of the microstructure during the cyclic deformation in-situ in a scanning electron microscope applying powerful techniques like electron-backscattered diffraction (EBSD) or electron channeling contrast imaging (ECCI). The nature and development of deformation bands, the phase transformation and the development of dislocation structures which are characteristic for fatigue (like planar and/or wavy dislocation arrangements etc.) are in the focus of this work.

2. Experimental

Flat specimens with geometry as shown in Fig. 1 and rectangular cross section of 5 × 2 mm² and a gauge length of 12 mm were prepared from heat treated high-alloyed cast TRIP-steel plates by milling. The chemical composition of the material investigated in the present study is given in Table 1. The microstructure of the cast steel shows a dendritic structure with large grains having grain diameters of 100 - 500μm obtained from optical light micrographs using line the intersection method.

Table 1. Chemical composition of the investigated cast TRIP steel (wt%)

C	Ni	Cr	Mn	Si	Al	N
0.06	5.70	15.20	5.46	0.96	0.09	0.06

Both specimen surfaces were carefully grinded and mechanically polished. The removed surface layer had a thickness of 250 μm. The specimens were tested in-situ in the vacuum chamber of a scanning electron microscope (Zeiss, DSM 960, tungsten cathode) using a spindle-driven push-pull loading stage (Kammrath&Weiss). The deformation rate is much smaller than in a servo-hydraulic push-pull machine. The motor velocity can be varied in a range between 1 to 20 μm/s. An extensometer measuring the total strain was mounted on the back side of the specimen. Fig. 2 shows the experimental setup on the SEM stage. Three cast TRIP steel specimens were deformed symmetrically in tension and compression (R= -1) at room temperature. Detailed testing programs are summarized in Table 2. The deformation was performed in total strain control with total strain amplitudes of $\varepsilon_{a,t} = 3 \times 10^{-3}$ and $\varepsilon_{a,t} = 5 \times 10^{-3}$. In-situ tests were interrupted at 100, 250 and 500 cycles corresponding to different stages of fatigue life N/N_f, where N_f is the fatigue life time. The in-situ tests were performed up to 100 cycles with a motor velocity of 10μm/s. After 100 cycles the motor velocity was increased to 20μm/s in order to reduce the measuring time inside the SEM. This results in total strain rates of $\dot{\varepsilon} = 1 \times 10^{-3}$ (10μm/s) and $\dot{\varepsilon} = 2 \times 10^{-3}$ (20μm/s) at the two applied total strain amplitudes. During the in-situ deformation SEM micrographs were taken using the back-scatter-electron (BSE)-contrast in order to see formation of deformation bands, orientation changes and places of phase transformation. Also secondary-electron (SE)-contrast was applied for several cycles in order to visualize changes in surface topography.

After 100, 250 and 500 cycles additional SEM investigations were carried out in a high-resolution SEM equipped with a field emission gun (FE-SEM) applying electron back-scatter-diffraction (EBSD) technique for analyzing the phase transformation and electron channelling contrast imaging (ECCI) for studying the developed dislocation arrangements. For this purpose the surface roughness due to cyclic deformation was polished away by slightly grinding (SiC-paper 4000) and subsequently short electro-polishing (8 s). EBSD measurements were done using CHANNEL5 from HKL (Oxford). ECCI was performed with a four-quadrant BSE detector at working distances ≤ 5 mm, large aperture (120 µm) and high beam current (HC-mode).

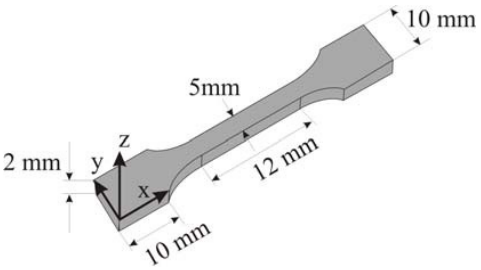

Fig. 1. Specimen geometry for in-situ deformation tests.

Fig.2. Push-pull loading stage with mounted specimen and extensometer on the backside of the specimen.

Table 2. Detailed testing program

	TRIP_A9	**TRIP_B2**	**TRIP_B4**
Test	Tension/compression	Tension/compression	Tension/compression
$\varepsilon_{a,t}$	5×10^{-3}	5×10^{-3}	3×10^{-3}
N	100 cycles	250, 500 cycles	250, 500 cycles
N/N_f	0.06	0.16, 0.33	0.02, 0.04

3. Results

3.1. In-situ cyclic deformation test

The in-situ cyclic deformation tests were carried out at two different total strain amplitudes $\varepsilon_{a,t} = 3 \times 10^{-3}$ and $\varepsilon_{a,t} = 5 \times 10^{-3}$. The tests were interrupted at defined deformation intervals and SEM-micrographs using back-scattered electrons (BSE) were taken for one individual area of interest of 100 × 100 µm.

Fig. 3 shows an example for specimen TRIP_A9 tested at $\varepsilon_{a,t} = 5 \times 10^{-3}$ after 1 cycle (a), 25 cycles (b), 50 cycles (c) and 100 cycles (d-g). From the BSE-signal micrographs it is clearly visible that the formation of deformation bands starts just from the beginning of cyclic deformation. Already after the 1st cycle (a) first deformation bands appear on three activated slip systems within one individual austenitic grain. They appear as straight, bright lines (marked by black arrows). Their density is increasing with increasing number of cycles. At the early beginning these bands are very fine and only visible in the orientation contrast using BSE signal. With increasing number of cycles these deformation bands are growing not only in length but also in thickness (b). With increasing thickness they start to grow out of the surface leading to a step-like surface profile (f, g). At a certain thickness of deformation bands dark, lentil-like irregularities can be observed inside the bright deformation bands indicated by black circles in (b) and (c). These irregularities start to form at this applied total strain amplitude between 20th and 30th cycle. They have a pronounced surface profile. Fig. 3(e) shows the topography of the marked area in (d) at higher magnification. It becomes also evident that deformation bands on different activated slip systems are different in thickness. Slip

bands of slip system 1 and 2 in Fig. 3(c) are much thicker than slip bands on slip system 3. This is assumed to be correlated with the different Schmid factors of the activated systems.

At 100 cycles the majority of grains show deformation bands on different activated slip systems with different thickness. One part of these grains shows already large areas correlated with phase transformation from fcc to bcc structure. The part of grains containing these phase transformation areas is increasing with ongoing cycling. At 250 cycles practically all grains show areas with phase transformation. Between 250 and 500 cycles these areas of phase transformation are growing as it is well illustrated in Fig. 4 for an individual grain in specimen TRIP_B2 at 250 cycles (a) and 500 cycles (b). The number of deformation bands or the band density seems to be unchanged (for instance in the area between the arrows). Only the areas of phase transformation are enlarging as shown by the marked areas.

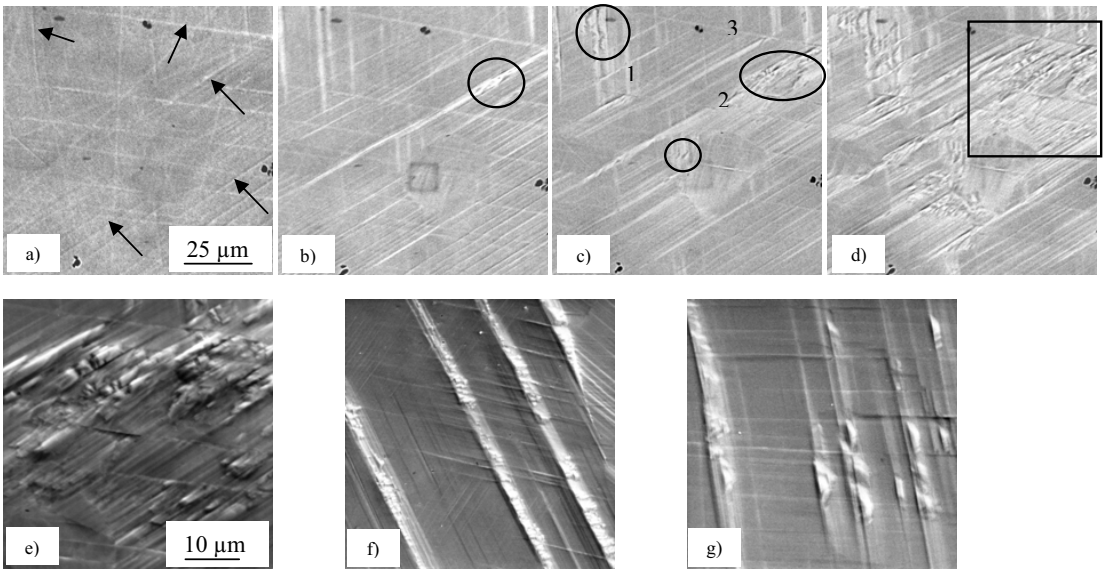

Fig. 3. In-situ SEM micrographs using backscattered electron signal of cast TRIP-steel specimen A9 cyclically deformed at $\varepsilon_{a,t} = 5 \times 10^{-3}$ at 1st cycle (a), 30th cycle (b), 50th cycle (c), 100th cycle (d) and using secondary electron signal at 100 cycles (e-g). Stress axis horizontal.

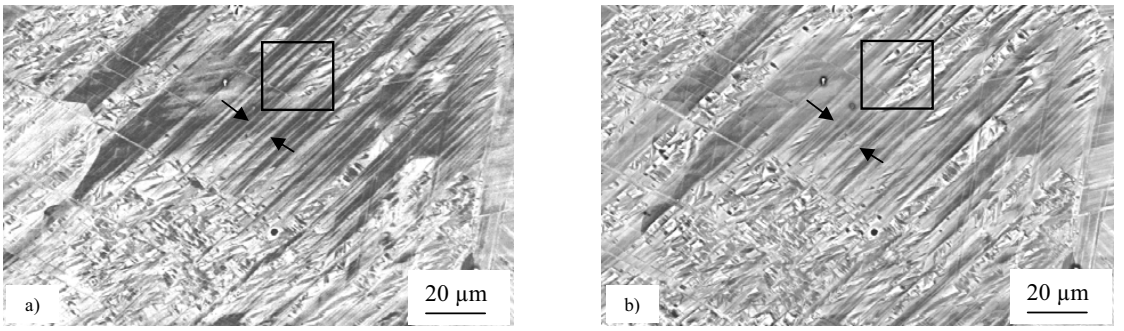

Fig. 4. FE-SEM micrographs using BSE signal of one individual grain in specimen TRIP_B2 cyclically deformed at $\varepsilon_{a,t} = 5 \times 10^{-3}$ up to 250 cycles (a) and 500 cycles (b). Stress axis horizontal.

For the lower total strain amplitude $\varepsilon_{a,t} = 3 \times 10^{-3}$ a similar behavior was observed. Deformation bands occur just from the beginning of cyclic deformation. But the growing in thickness with increasing number of cycles is much smaller than observed at higher total strain amplitudes. Fig. 5 shows an example for an individual grain in specimen

TRIP_B4 deformed at $\varepsilon_{a,t} = 3 \times 10^{-3}$ up to 250 (a) and 500 cycles (b). The micrographs were taken using the BSE signal and show clearly the changes in the developing microstructure. Although deformation bands are very thin after 250 cycles few places of phase transformation can be already observed (marked by arrows). These areas are growing with ongoing cyclic deformation, whereas the number of observed deformation bands remains unchanged.

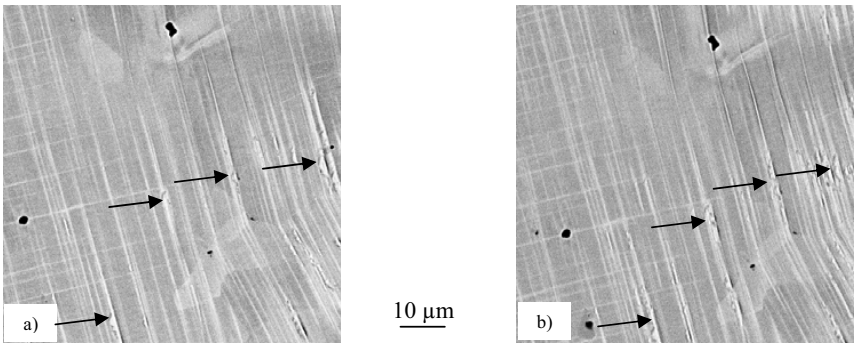

Fig. 5. SEM micrographs using BSE signal of an individual grain in cast TRIP-steel specimen B4 cyclically deformed at $\varepsilon_{a,} = 3 \times 10^{-3}$ up to 250 (a) and 500 cycles (b), respectively. Stress axis horizontal.

3.2. Phase transformation and microstructure

In order to investigate the microstructure forming processes as well as the phase transformation from the austenitic γ-phase with fcc structure into the α'-martensite phase with a bcc structure EBSD measurements and ECCI investigations were performed. In the following the results for cyclic deformation with two different total strain amplitudes at different number of cycles are described.

Microstructures for $\varepsilon_{a,t} = 5 \times 10^{-3}$ at 100, 250 and 500 cycles

Fig. 6 shows the EBSD results for an individual austenitic grain deformed up to 100 cycles. The map was performed with a grid of 250 × 200 points and a step width of 0.2 µm. For indexing of Kikuchi lines the match units of fcc iron (red), bcc iron (blue) and hcp iron (yellow) were used. Fig. 6 (a) shows the phase identification map. It can be clearly seen that in this area deformation bands on two different slip systems were detected. These deformation bands show different thicknesses. The major part of the observed deformation bands was indexed with a hexagonal crystal structure. Many areas with bcc structure corresponding to the α'-martensite were found within these bands of hexagonal crystal structure. It is interesting that α'-martensite was detected not only in the very thick bands of the primary slip system. Also in the very thin bands of the secondary slip system α'-martensite was formed. Fig. 6 (b) shows the crystal orientation map of the investigated area. The coloring corresponds to the inverse pole figure of the loading axis which lies horizontal in all figures. The austenitic grain has a uniform orientation close to <111> direction parallel to the loading axis. The formed α'-martensite grains show different crystallographic orientations corresponding to different variants of α'-martensite. The orientation relationship between the fcc, bcc and hcp phases are explained by Fig. 6 (c) and (d). Fig. 6 (c) shows the band contrast image overlapped by the crystallographic orientations of the bcc phase. Additionally, the fcc/bcc phase orientation relationship after Kurdjumov and Sachs [8] $\{111\}_\gamma \parallel \{110\}_{\alpha'}$ and $<110>_\gamma \parallel <111>_{\alpha'}$ is indicated by white lines. The boundaries between different variants of α'-martensite correspond mainly to 60°<111> (Σ3, red lines) boundaries. But also boundaries with a misorientation axis/angle pair of 50°<110> (Σ11, yellow lines) were observed. Fig. 6 (d) shows the band contrast images overlapped by the crystallographic orientation of the hcp structure. The hexagonally indexed areas have contrary to the bcc structure a uniform crystallographic orientation. The orientation relationship fcc/hcp structure $\{111\}_\gamma \parallel \{001\}_\varepsilon$ [9] is indicated by white lines and the orientation relationship hcp/bcc structure $\{001\}_\varepsilon \parallel \{110\}_{\alpha'}$ by yellow lines. Furthermore, in the band contrast image Fig. 6 (d) a lot of deformation bands can

be recognized which were not indexed as hexagonal structure but as fcc structure with the same orientation as the austenitic “mother” grain.

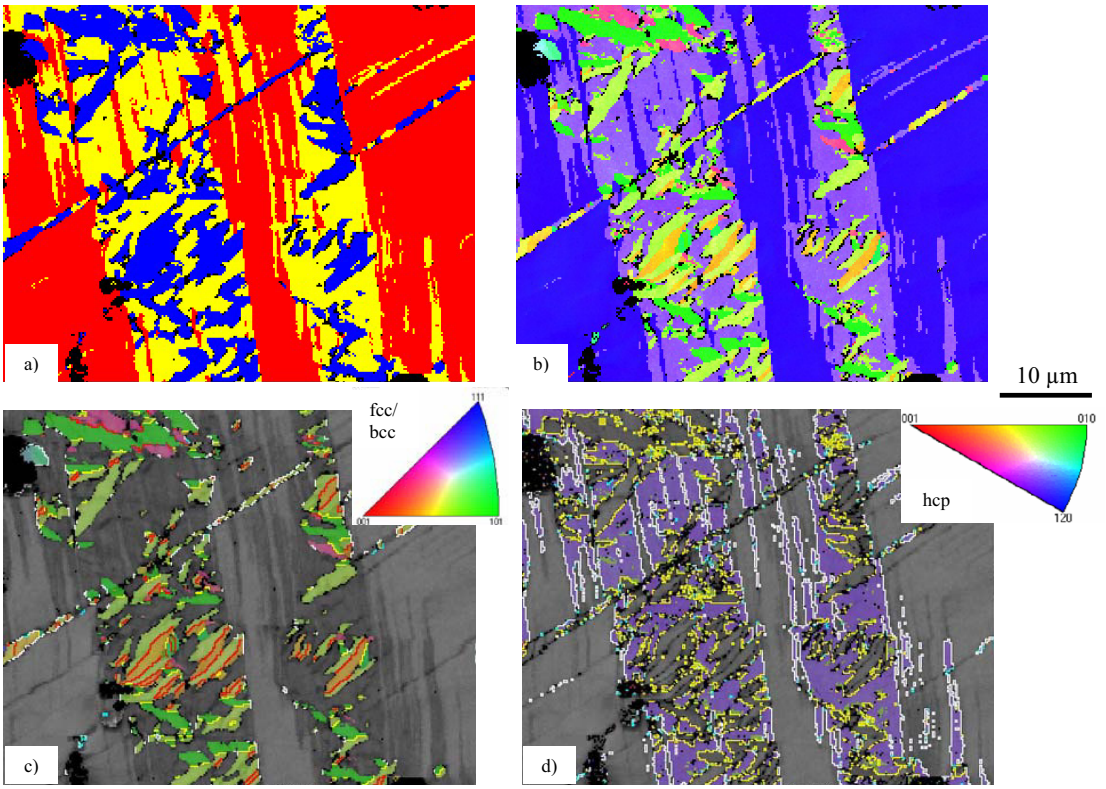

Fig. 6. EBSD results obtained on a cast TRIP-steel specimen cyclically deformed at $\varepsilon_{a,t} = 5 \times 10^{-3}$ up to 100 cycles. (a) Phase identification, red … fcc (γ-phase), yellow…hcp, blue…bcc (α’-phase), black…zero solutions. (b) Combined orientation map for fcc (γ-phase), bcc (α’-phase) and hcp (ε-phase) structures. (c) Band contrast overlapped by bcc orientation map with indicated lattice orientation relationship fcc/bcc structure (white lines) and grain boundary relationships within bcc structure (red, yellow lines). (d) Band contrast overlapped by hcp orientation map with indicated lattice orientation relationships fcc/hcp (white lines) and bcc/hcp (yellow lines).

The electron channeling contrast imaging is a powerful technique for the investigation of the developed dislocation structure in a scanning electron microscope. Using high-resolution FE-SEM it is even possible to investigate individual dislocations and stacking faults [10]. Regarding the developed dislocation arrangement at $\varepsilon_{a,t} = 5 \times 10^{-3}$ after 100 cycles two different features can be distinguished which are well illustrated in Fig. 7 for four individual grains. The observed deformation bands developing from the first cycle consist of many very thin, parallel, straight lamellas Fig. 7 (a). These lamellas develop on all activated slip systems and are different in length (a, b). Long extended lamellas are observed on two slip systems as well as short parts lying parallel between the long extended lamellas. They are correlated with dislocations, because due to slightly tilting around one specimen axis it is possible to bring them out of contrast (like g × b criterion in TEM). In some grains the formation of a dislocation cell structure was detected as shown in Fig. 7 (c) and (d). Dislocation cells are formed both between deformation bands (c) as well as in areas which are free of deformation bands (d). The formation of the cell structure is just at the beginning and cells are not well pronounced at this state. The cell walls are not as sharp as it was observed at the end of fatigue life (see [6, 7]).

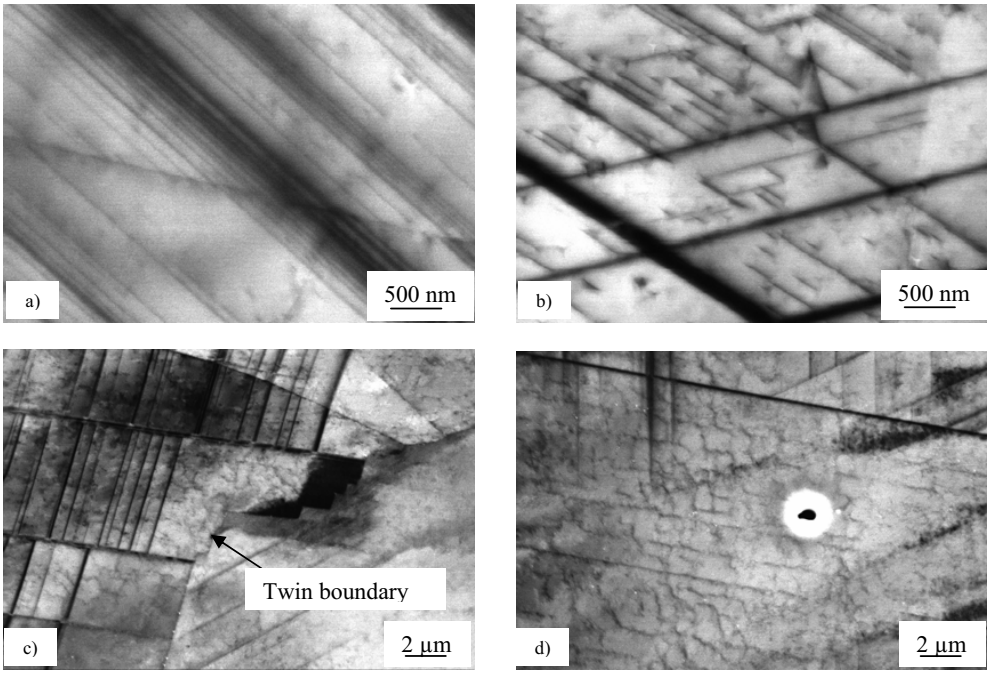

Fig. 7. Inverted ECC-images of four individual grains in high-alloyed cast TRIP-steel specimen A9 deformed at $\varepsilon_{a,t} = 5 \times 10^{-3}$ up to 100 cycles. (a) High magnification of individual deformation bands showing lamellar structure. (b) Short lamellas lying parallel to deformation bands on different activated slip systems. (c) Two grains separated by a (incoherent) twin boundary. The left grain contains intersecting deformation bands, the right grain only deformation bands on one slip system, between deformation bands a dislocation cell structure starts to develop. (d) Dislocation cell structure. Stress axis horizontal.

Fig. 8 shows the results of EBSD measurements on the same individual grain as shown in Fig. 4 deformed with $\varepsilon_{a,t} = 5 \times 10^{-3}$ up to 250 and 500 cycles. A comparison of the phase maps at 250 and 500 cycles demonstrates quite well that practically no new deformation bands formed during 250 additional cycles. Instead, deformation bands already existing at 250 cycles which were still indexed as fcc structure changed now into the hexagonal structure (marked by white arrows). In addition deformation bands which had already at 250 cycles a hexagonal structure show more and more areas with bcc lattice structure of α'-martensite (see white circles).

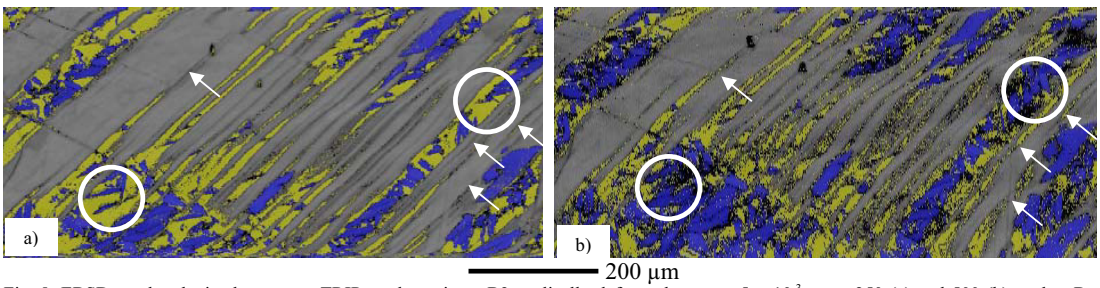

Fig. 8. EBSD-results obtained on a cast TRIP-steel specimen B2 cyclically deformed at $\varepsilon_{a,t} = 5 \times 10^{-3}$ up to 250 (a) and 500 (b) cycles. Band contrast image with overlapped phase identification; yellow…hcp, blue…bcc (α'-phase), rest fcc (γ-phase), black…zero solutions.

Within the area of interest the fraction of α'-martensite increases significantly from 13 % at 250 cycles up to 20 % at 500 cycles whereas the fraction of hexagonally indexed structure remains nearly unchanged (21% at 250 cycles and 20% at 500 cycles). At the same time, the γ-phase is reducing from 60% to 50%. Thus, deformation bands with

a hexagonal structure at 250 cycles transform to α'-martensite and bands with a fcc structure at 250 cycle transform to hcp structure. Furthermore it can be seen that the fraction of zero solutions (non indexed Kikuchi-pattern) increases from 4% to 11%. The reason for that could be the surface roughness which developed during the 250 additional cycles and which was not removed before the second EBSD measurement.

Fig. 9 illustrates the evolution of the dislocation arrangement between 250 (a) and 500 cycles (b) for the same grain shown already in Fig. 4 and 8. The lamellar structure of the deformation band in the centre of the micrograph can be clearly revealed from the inverted ECC images both after 250 and 500 cycles. The thickness of the central deformation band (about 600 nm) has not changed remarkably during the 250 additional cycles. Likewise, the lamella nearly perpendicular to the loading axis remains unchanged. A closer look on the left side of the central deformation band (marked by white ellipse) reveals that in this region a new lamella was developed between 250 and 500 cycles. Furthermore, some of them are grown in length. In addition, at 500 cycles the deformation band in the upper left corner shows areas of phase transformation (white arrows).

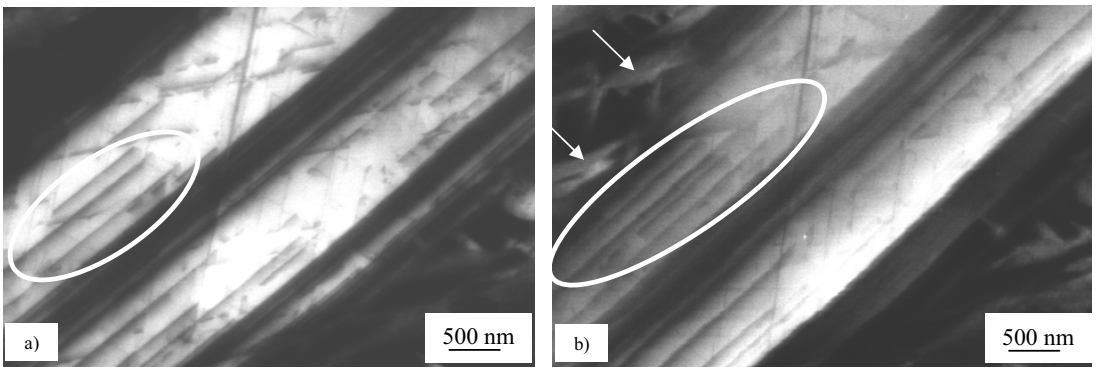

Fig. 9. Inverted ECC images showing changes in the dislocation arrangement within the same individual grain as shown in Figs. 4 and 8 between 250 (a) and 500 cycles (b).

Microstructures for $\varepsilon_{a,t}$ =3 × 10^{-3} at 250 cycles

Fig. 10 shows the results of EBSD measurements (a) and the dislocation arrangement in the same grain already shown in Fig.5 at 250 cycles.

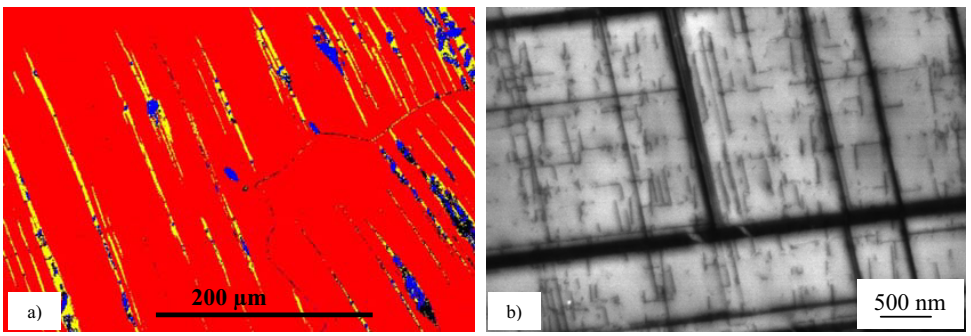

Fig. 10. Microstructures observed on cast TRIP-steel specimen B4 cyclically deformed at $\varepsilon_{a,t}$ = 3 × 10^{-3} up to 250 cycles. (a) EBSD-phase identification map - red… fcc (austenite, γ-phase), yellow…hcp, blue…bcc (α'-phase). (b) Inverted ECC images showing intersection of deformation bands on two different activated slip systems. Short lamellas parallel to the two sets of deformation bands are visible.

It can be clearly seen that at the lower total strain amplitude the martensitic phase transformation is not so pronounced as at the higher total strain amplitude (compare Fig. 8a and Fig. 10a). Only few deformation bands were indexed by hexagonal structure. The fraction of α'- martensite and hexagonally indexed structure are quite low with

2% for α'-martensite and 5% for hexagonal structure, respectively, in the measured grid (500 × 400 points, step width of 1 μm).

At 250 cycles, the dislocation arrangement shows planar slip without exception. In Fig. 10 (b) intersecting deformation bands on two different activated slip systems are visible. The deformation bands consist again of a fine lamellar structure. Shorter parts of such lamellas were observed again parallel to the well pronounced deformation bands.

4. Discussion

The in-situ and pseudo-in-situ (EBSD, ECCI) observed evolution of the microstructure correlates very well with the cyclic deformation behavior of this type of high-alloyed TRIP-steel described in [7]. The authors reported a pronounced hardening behavior for total strain amplitudes $\varepsilon_{a,t} \geq 2.0 \times 10^{-3}$ which is an indicator for the occurrence of martensitic phase transformation [11]. Accompanying measurement of the evolution of the ferromagnetic phase fraction during the cyclic deformations manifests the formation of ferromagnetic α'-martensite as the reason for hardening. With the onset of hardening the first α'-martensite was detected by ferritscope for $\varepsilon_{a,t} = 3 \times 10^{-3}$ at about 500 cycles and for $\varepsilon_{a,t} = 5 \times 10^{-3}$ at 100 cycles. Increasing total strain amplitude leads to a shorter incubation time for the martensitic transformation. The observation of the microstructure during in-situ deformation in the SEM at $\varepsilon_{a,t} = 3 \times 10^{-3}$ and $\varepsilon_{a,t} = 5 \times 10^{-3}$ showed that the martensitic transformation starts very locally already earlier at about 30 cycles for the higher total strain amplitude and at about 100 cycles for the smaller ones.

The EBSD measurements for two different total strain amplitudes at different number of cycles revealed that the deformation-induced phase transformation in the presently investigated high alloyed cast TRIP steel takes place by transformation of the austenitic fcc γ-phase into the bcc α'-martensite phase via an intermediate hexagonal crystal structure. The detected lattice relationship $\{111\}_\gamma \parallel \{001\}_\varepsilon \parallel \{110\}_{\alpha'}$ and $<110>_\gamma \parallel <120>_\varepsilon \parallel <111>_{\alpha'}$ is in good agreement with the literature [8, 9]. α'-martensite forms also within deformation bands and not only at intersection points of deformation bands of different slip systems.

The hexagonal structure within deformation bands was also detected by many other authors [12-20]. However, different reasons were given, i.e. deformation twinning or formation of stacking faults. The presently investigated high-alloyed TRIP steel has a high content of manganese leading to significantly reduced stacking fault energy. In steels with high stacking fault energy – so called TWIP steels – no deformation induced phase transformation takes place, but the formation of micro- or nano twins [12, 13, 14, 15]. In [13, 16] models are described for steels with medium stacking fault energy where at lower stresses the formation of stacking faults dominates and with increasing stresses the stacking faults tend to overlap and to form twins. The present high-alloyed TRIP steel has a SFE of 25 mJ/m³ (calculated, see [7]). From the EBSD measurements as well as the ECCI investigations it is obvious that in the present case the occurring deformation mechanism is the splitting of dislocations into Shockley partials forming stacking faults. Buyn et al. [17-20] describe that the distance of Shockley partials or the width of faulted regions can enlarge with increasing plastic deformation and patches of extended stacking faults fringes can be observed along {111} slip planes.

The observed dislocation arrangement is in agreement with results from the literature [21, 22] where transition from planar to wavy glide behavior is reported with increasing total strain amplitude. In the present study, a dislocation cell structure was observed already very early in the fatigue life for $\varepsilon_{a,t} = 5 \times 10^{-3}$.

At the investigated earlier stages of fatigue life no formation of classic extrusion/intrusion profiles or persistent slip bands was observed. Furthermore, no crack initiation was detected neither on pores and precipitates of the cast material nor on the formed α'-martensite up to 0.33 N_f.

5. Conclusions

In the present work the evolution of the microstructure during cyclic deformation of a high-alloyed TRIP steel was investigated in-situ in scanning electron microscopy for two different applied total strain amplitudes at early stages of fatigue life. The following conclusions can be drawn:

(1) Formation of deformation bands during cyclic deformation starts very early in the fatigue life.

(2) At a certain thickness these deformation bands were indexed by a hexagonal crystal structure.

(3) Formation of α'-martensite starts always inside the deformation bands with a hexagonal structure and not only at intersection points of deformation bands.
(4) The inner structure of deformation bands exhibits a lamellar structure. Shorter parts of such lamellas were found always parallel to pronounced deformation bands on different activated slip systems.
(5) The nature of this lamellar structure are stacking faults produced by separation of dislocations in Shockley partials.

Main points of interest for further investigations are: (i) effect of grain size and grain orientation as well as segregations on the martensitic phase transformation and the occurring microstructure evolution processes, (ii) favored places for fatigue damage (crack initiation, crack propagation) and (iii) determination of local strain fields by digital image correlation.

Acknowledgement

The authors thank the German Research Foundation for the financial support of the Collaborative Research Centre "TRIP-Matrix-Composites" (SFB 799).

References

[1] H. Biermann, C. G. Aneziris, M. Kuna: Collaborative Research Center TRIP-Matrix-Composite, Proc. of ESOMAT 2009, DOI:10.1051/esomat/200905002.

[2] A. Weiß, H. Gutte, M. Radke, P. Scheller, patent specification WO002008009722A1.

[3] C. G. Aneziris, W. Schärfl, H. Biermann, U. Martin: Energy absorbing TRIP-steel/Mg-PSZ composite-honeycomb structures based on ceramic extrusion at room temperature, Int. J. Appl. Ceramic Techn. 2009; 6: 727-35.

[4] H. Biermann, U. Martin, C.G. Aneziris, A. Kolbe, A. Müller, W. Schärfl et al.: Microstructure and compression strength of novel TRIP-steel/Mg-PSZ composites, Adv. Eng. Mater. 2009; 11: 1000-6.

[5] S. Martin, S. Wolf, U. Martin, L. Krüger, A. Jahn: Investigations on martensite formation in CrMnNi-TRIP steels. Proc. of ESOMAT 2009, DOI:10.1051/esomat/200905022.

[6] A. Glage, A. Weidner, T. Richter, P. Trubitz, H. Biermann: Low cycle fatigue behavior and microstructure of a high alloyed metastable austenitic cast TRIP-steel. Proc. of ESOMAT 2009, DOI:10.1051/esomat/200905007.

[7] A. Glage, A. Weidner, H. Biermann: Effect of austenite stability on the low cycle fatigue behavior and microstructure of high alloyed metastable austenitic cast TRIP-steels. Proc. of Fatigue conference 2010, Prague, Procedia Engineering 2010.

[8] G. Kurdjumov, G. Sachs: On the mechanism of steel hardening. Mitteilung Kaiser Wilhelm-Institut für Metallforschung 1935: 325-43.

[9] H. Schumann: Zur Kristallographie der ε-α-Gitterumwandlung, Kristall und Technik 1976; 11: 663-71.

[10] B. A. Simkin, B-C. Ng, M.A.Crimp, Imaging crystalline defects in the SEM by electron channeling contrast, Micros.Anal.1999; 77:11-3.

[11] U. Krupp, C. West, H. -J. Christ: Deformation-induced martensite formation during cyclic deformation of metastable austenitic steel: Influence of temperature and carbon content. Mater. Sci. Eng. A 2008; 481-482: 713-17.

[12] I. Gutierrez-Urrutia, S. Zaefferer, D. Raabe: Electron channeling contrast imaging of twins and dislocations in twinning-induced plasticity steels under controlled diffraction conditions in a scanning electron microscope. Scripta Mater. 2009; 61: 737-40.

[13] T. H. Lee, C. S. Oh, S.J. Kim, S.Takaki: Deformation twinning in high-nitrogen austenitic stainless steel. Acta Mater. 2007; 55: 3649-62.

[14] K. Verbeeken, N. van Caenegam, M. Verhaege: Quantification of the amount of ε - martensite in a Fe–Mn–Si–Cr–Ni shape memory alloy by means of electron backscatter diffraction. Mater. Sci. Eng. A 2008; 481-482: 471-75.

[15] L. Bracke, K. Verbeeken, L. Kestens, J. Penning: Microstructure and texture evolution during cold rolling and annealing of a high Mn TWIP steel. Acta Mater. 2009; 57: 1512-24.

[16] J. Talonen, H. Hänninen: Formation of shear bands and strain-induced martensite during plastic deformation of metastable austenitic stainless steels. Acta Mater. 2007; 55: 6108-18.

[17] T.S. Buyn, E. H. Lee, J.D. Hunn, Plastic deformation in 316LN steel – characterization of deformation microstructures. J. Nucl. Mater. 2003; 321: 29-39.

[18] T. S. Buyn: On the stress dependence of partial dislocation separation and deformation microstructure in austenitic stainless steels. Acta Mater. 2003; 51: 3063-71.

[19] N. Hashimoto, T.S. Byun: Deformation induced martensite formation and dislocation channeling in neutron-irradiated 316 stainless steel. J. Nucl. Mater. 2007; 367-370: 960-65.

[20] E.H. Lee, T.S. Byun, J.D. Hunn, K. Farrell, L.K. Mansur: Origin of hardening and deformation mechanisms in irradiated 316 LN austenitic stainless steel J. Nucl. Mater. 2001; 296: 183-191.

[21] T. Kruml, J. Polák, K. Obrtlík, S. Degallaix: Dislocation structures in the bands of localised cyclic plastic strain in austenitic 316L and austenitic-ferritic duplex stainless steels, Acta Mater. 1997; 45: 5145-51.

[22] Y. Kaneko, K. Fukui, S. Hashimoto: Dislocation structures around crack tips of fatigued polycrystalline copper, Mater. Sci. Eng. A 2005; 400-401: 413-19.